Frontiers of Information Technology & Electronic Engineering
www.jzus.zju.edu.cn; engineering.cae.cn; www.springerlink.com
ISSN 2095-9184 (print); ISSN 2095-9230 (online)
E-mail: jzus@zju.edu.cn

Intelligent fractional-order integral sliding mode control for PMSM based on an improved cascade observer*

Lingfei XIAO†‡[1,2], Leiming MA[3], Xinhao HUANG[1]

[1]*College of Energy and Power Engineering, Nanjing University of Aeronautics and Astronautics, Nanjing 210016, China*

[2]*State Key Laboratory of Fluid Power and Mechatronic Systems, Zhejiang University, Hangzhou 310027, China*

[3]*College of Automation Engineering, Nanjing University of Aeronautics and Astronautics, Nanjing 210016, China*

†E-mail: lfxiao@nuaa.edu.cn

Received July 3, 2020; Revision accepted June 13, 2021; Crosschecked Nov. 19, 2021

Abstract: In this paper, an intelligent fractional-order integral sliding mode control (FOISMC) strategy based on an improved cascade observer is proposed. First, an FOISMC strategy is designed to control a permanent magnet synchronous motor. It has good tracking performance, is strongly robust, and can effectively reduce chattering. The proposed FOISMC strategy associates strong points of the integral action (which can eliminate steady-state tracking errors) and the fractional calculus (which is flexible). Second, an improved cascade observer is proposed to detect the rotor information with a smaller observation error. The proposed observer combines an adaptive sliding mode observer and an extended high-gain observer. In addition, an improved variable-speed grey wolf optimization algorithm is designed to enhance controller parameters. The effectiveness of the strategy is tested using simulations and an experiment involving model uncertainty and external disturbance.

Key words: Permanent magnet synchronous motor; Fractional-order integral sliding mode; Optimization algorithm; Sensorless control; Observer

https://doi.org/10.1631/FITEE.2000317 **CLC number:** TK83; TN06

1 Introduction

Because of its high efficiency, high torque density, and good reliability, the permanent magnet synchronous motor (PMSM) has been used in many applications and has attracted much attention from researchers (Wang et al., 2018). The control effect is closely related to the rotor information. However, traditional position sensors cause many control system stability problems. Consequently, many scholars have focused on sensorless control research (Wu and Zhang, 2018).

Sensorless strategies include high-frequency signal injection methods (Foo and Rahman, 2010), direct torque control (DTC) methods (Wang et al., 2018), and observer methods (Wu and Zhang, 2018). Xie et al. (2018) considered a sliding mode control (SMC) method with an extended state observer and achieved significantly reduced chattering and increased robustness. A disturbance observer (DOB) has been applied (Yan et al., 2019), and the results showed that the scheme is able to suppress disturbance. A fractional-order terminal SMC method was designed to improve the control effect (Fei and Feng, 2020; Fei and Wang, 2020). The improved neural network was used to estimate an active power filter and micro gyroscope model (Fei and Chen, 2020; Fei and Feng, 2020). The simulation results showed that the proposed control strategy could improve tracking performance. In the above studies, model

‡ Corresponding author

* Project supported by the National Natural Science Foundation of China (No. 51876089) and the Open Foundation of the State Key Laboratory of Fluid Power and Mechatronic Systems, China (No. GZKF-202005)

ORCID: Lingfei XIAO, https://orcid.org/0000-0003-0255-1124; Leiming MA, https://orcid.org/0000-0001-5831-959X

uncertainty and external disturbances were not considered simultaneously.

With further study of the fractional calculus theory in recent years, fractional-order SMC has gradually become an important branch of SMC. Fractional-order proportional-integral (PI) was used to replace traditional PI, and the load torque was estimated by DOB (Apte et al., 2019). The results showed that the proposed strategy has better control performance. The integer- and fractional-order models of the PMSM were compared by Thakar et al. (2017). The results showed that the fractional-order PMSM model can obtain better control performance. In addition, the hybrid of an intelligent optimization algorithm and fractional calculus has become the focus of research. A fractional-order fuzzy control strategy was proposed by Pan and Das (2016), and a particle swarm optimization (PSO) algorithm was applied. A fuzzy neural network was employed by Fei and Feng (2020), and the fractional calculus was combined with super-twisting SMC to effectively improve the control performance. The fractional operator can be mathematically defined using the Riemann-Liouville definition (Bakkyaraj and Sahadevan, 2015), Grünwald-Letnikov definition (MacDonald et al., 2015), and Caputo definition (Waheed et al., 2019). The controller is designed based on Riemann-Liouville fractional calculus in this study. Fractional-order integral SMC (FOISMC) is applied to control PMSM, and good tracking performance, strong robustness, and effective chatter reduction are achieved.

An adaptive high-gain observer (HGO) was proposed by Hamida et al. (2017) and was used to estimate the rotor information. Nguyen et al. (2018) proposed a model reference adaptive control (MRAC) strategy, which ensured stability and realized accurate speed tracking. Multi-parameter estimation with MRAC was designed by Kivanc and Ozturk (2018), which mitigated the effect of multiple parameters at a low speed and improved the dynamic performance. In summary, the DOB (Kivanc and Ozturk, 2018; Yan et al., 2019), sliding mode observer (SMO) (Yang et al., 2019), HGO (Hamida et al., 2017), MRAC (Nguyen et al., 2018), and extended Kalman filter (Shi et al., 2015) have been employed in PMSM control. In recent years, many improved SMOs have been studied. An adaptive SMO (ASMO) was employed to improve the observation effect (Zhao et al., 2013). A fuzzy SMO (FSMO) was designed by Zhang et al. (2014), which improved the robustness of the SMO. In this study, a cascade observer, based on an ASMO and extended high-gain observer (EHGO), was used to observe PMSM information.

The FOISMC strategy can effectively reduce chattering, but the number of adjustable parameters will increase. It is extremely difficult to manually adjust the controller parameters. Some conventional gradient-based optimization methods, such as the Newton method and interior point method, have been proposed, but these optimization methods may fail to determine the optimal parameters because of their high dependence on an accurate system model. Hence, several heuristic algorithms have been developed to overcome the above challenges, such as PSO and grey wolf optimization (GWO). These optimization algorithms can achieve efficient global search with lower dependence on an accurate system model. Typical swarm intelligence optimization algorithms include PSO (Poli et al., 2007), GWO (Mirjalili et al., 2014), and artificial bee colony (ABC) (Tran et al., 2015). The heuristic optimization algorithm has been studied to overcome the problems of function optimization and clustering optimization, because of its simple structure and few adjustable parameters. PSO was used to ensure the maximum wind energy extraction by adjusting controller parameters (Bakkyaraj and Sahadevan, 2015). The main advantages of PSO are its strong global search ability, simple principles, and high convergence speed, while the main disadvantages are poor local search ability and low search accuracy. Recently, GWO has been widely used, and the location of the prey is the solution to the corresponding problem. The research results showed that GWO is better than PSO and genetic algorithms in searching for a global optimal solution. GWO has the advantages of high convergence speed and strong local search ability, but there are some problems, such as insufficient global search ability, low solution accuracy, and low convergence speed in the later stages of optimization (Mirjalili et al., 2014). These algorithms have their own advantages. Better results can be achieved when the advantages of these different algorithms are combined. A hybrid of GWO and the differential evolution (DE) algorithm was proposed by Zhu et al. (2015), which used GWO to strengthen the local

optimization ability and DE to improve the global search effect. The variable-speed GWO (VGWO) presented in this study, with high convergence speed, high solution accuracy, and strong global optimization ability, realizes parameter optimization of the wind turbine torque controller. Similar research ideas were adopted by Ma et al. (2021).

Remark 1 Compared with Ma et al. (2021), in this study the differences and advantages of the controller, observer design, and optimization algorithm are mainly as follows:

1. Controller design

In this study, FOISMC is adopted due to the flexibility and memory effect of fractional calculus, which can improve the accuracy of the controller, while Ma et al. (2021) used the integral action of the second-order integral SMC (SOISMC) to reduce chattering. Although the proposed SOISMC strategy (Ma et al., 2021) has been widely studied, the FOISMC used in this study is a research hot field at present, and there are many topics worth exploring.

2. Observer design

Combining the advantages of the cascade observer designed by Ma et al. (2021), an ASMO with a high observation accuracy is designed in this study. Compared with the direct sliding mode observer (DSMO) designed by Ma et al. (2021), the ASMO uses more PMSM information, creating a significant improvement in observation accuracy.

3. Optimization algorithm

Fractional calculus is introduced into the controller designed in this study, and its parameter ranges from 0 to 1. The wide magnitude of the main adjustable parameters of the proposed control strategy brings challenges to the optimization algorithm. We further verify the effectiveness of the VGWO algorithm by increasing the number of iterations.

In this paper we propose an intelligent FOISMC strategy which is based on an improved cascade observer. The primary contributions can be summarized as follows:

1. An intelligent FOISMC strategy is designed that has good tracking performance and combines strong points of ISMC in eliminating steady-state tracking errors and the flexibility of fractional calculus.

2. An improved cascade observer is proposed based on an ASMO and EHGO, and is used to effectively observe the rotor information with higher observation accuracy.

3. Considering both the model parameter and load torque changes, the strategy can achieve accurate rotor speed tracking.

Finally, the strategy is implemented based on Simulink and the experimental system.

Notations In this paper, without special illustration, $\|\cdot\|$ represents the 2-norm of a matrix or a vector. For a real matrix or a vector M, $M>0$ ($M\geq 0$) means that all its entries are positive (nonnegative). $|\cdot|$ represents absolute value. Range, Max, Mean, and Std represent the variation range, maximum, mean, and standard deviation of the corresponding variables, respectively. D is the derivative operator. The variables with subscripts "$\wedge$" and "$\sim$" represent the estimate and the estimation error, respectively.

2 Uncertain PMSM model

For the mathematical model of PMSM, readers can refer to Ma et al. (2021). The uncertain PMSM model is introduced mainly as

$$\dot{x}_i = A_i x_i + B_i u_i + g_i(t), \tag{1a}$$

$$\dot{\omega} = A_\omega \omega + B_\omega u_\omega + g_\omega(t), \tag{1b}$$

where $g_i(t) = [g_{id}(t), g_{iq}(t)]^{\mathrm{T}} = \Delta A_i x_i + \Delta B_i u_i + d_i + \Delta d_i$ and $g_\omega(t) = \Delta A_\omega \omega + \Delta B_\omega u_\omega + d_\omega + \Delta d_\omega$, which are the lumped disturbances. ω is the mechanical rotor speed. The specific meanings of these parameters can be seen in Ma et al. (2021).

Assumption 1 $g_i(t)$ and $g_\omega(t)$ are continuous and satisfy $\|\dot{g}_{id}(t)\|\leq D_d$, $\|\dot{g}_{iq}(t)\|\leq D_q$, and $\|\dot{g}_\omega(t)\|\leq D_\omega$, where D_d, D_q, and D_ω are the known positive constants.

Integrating Eqs. (1a) and (1b), we obtain the following equation:

$$\dot{x} = Ax + Bu + g(t), \tag{1c}$$

where $x=[x_i,\omega]^{\mathrm{T}}$, $A=\mathrm{diag}(A_i, A_\omega)$, $u=[u_i,u_\omega]^{\mathrm{T}}$, $B=\mathrm{diag}(B_i,B_\omega)$, and $g(t)=[g_i(t),g_\omega(t)]^{\mathrm{T}}$.

3 Intelligent FOISMC design

The control structure is shown in Fig. 1. These controller parameters are adjusted using VGWO.

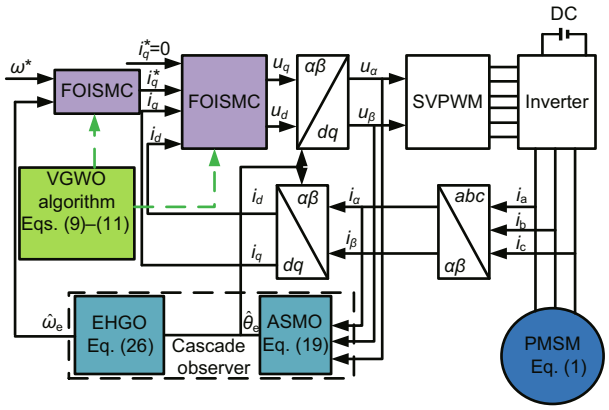

Fig. 1 The proposed control structure of PMSM (SVPWM: space vector pulse width modulation)

3.1 FOISMC design

3.1.1 Design of sliding mode surface

The tracking errors are defined as

$$\begin{bmatrix} e_{i_d} \\ e_{i_q} \\ e_\omega \end{bmatrix} = \begin{bmatrix} i_d^* - i_d \\ i_q^* - i_q \\ \omega^* - \omega \end{bmatrix}, \tag{2a}$$

where i_d^* and i_q^* are the d- and q-axis reference currents respectively, and ω^* is the reference rotor speed.

Considering $e = [e_{i_d}, e_{i_q}, e_\omega]^{\mathrm{T}}$ and $x^* = [i_d^*, i_q^*, \omega^*]^{\mathrm{T}}$, we have

$$e = x^* - x. \tag{2b}$$

Based on Eqs. (2a) and (2b), let $s = [s_d, s_q, s_\omega]^{\mathrm{T}}$ be the fractional-order integral sliding mode vector. The sliding mode surface s of the FOISMC is as follows:

$$s = \alpha e + \beta D^{-\varepsilon} e, \tag{3}$$

where $\alpha = \mathrm{diag}(\alpha_{i_d}, \alpha_{i_q}, \alpha_\omega)$ and $\beta = \mathrm{diag}(\beta_{i_d}, \beta_{i_q}, \beta_\omega)$ are the positive diagonal matrices, which can be chosen by ensuring the convergence rate of the tracking error. $\varepsilon = \mathrm{diag}(\varepsilon_{i_d}, \varepsilon_{i_q}, \varepsilon_\omega)$ is the order of fractional calculus, and $0 < \varepsilon_{i_d}, \varepsilon_{i_q}, \varepsilon_\omega < 1$.

Hence, the sliding mode manifold is $S_{\mathrm{FOISMC}} = \{e | s = \dot{s} = 0\}$.

3.1.2 Controller design

The derivation of s is obtained as

$$\begin{aligned} \dot{s} &= \beta D^{1-\varepsilon} e + \alpha \dot{e} = \beta D^{1-\varepsilon} e + \alpha(\dot{x}^* - \dot{x}) \\ &= \beta D^{1-\varepsilon} e + \alpha[\dot{x}^* - Ax - Bu - g(t)]. \end{aligned} \tag{4}$$

The control law u is

$$u = u_{\mathrm{eq}} + u_{\mathrm{sw}}. \tag{5a}$$

Overlooking the uncertainty and disturbance, the equivalent control law u_{eq} is

$$u_{\mathrm{eq}} = (\alpha B)^{-1}[\beta D^{1-\varepsilon} e + \alpha \dot{x}^* - \alpha A x]. \tag{5b}$$

The switching control law u_{sw} is

$$u_{\mathrm{sw}} = (\alpha B)^{-1}[k_1 s + k_2 D^{\gamma} \mathrm{sgn}(s)], \tag{5c}$$

where $\gamma = \mathrm{diag}(\gamma_{i_d}, \gamma_{i_q}, \gamma_\omega)$, $k_1 = \mathrm{diag}(k_{i1d}, k_{i1q}, k_{\omega 1})$, and $k_2 = \mathrm{diag}(k_{i2d}, k_{i2q}, k_{\omega 2})$.

Let $\Phi = \beta D^{1-\varepsilon} e + \alpha \dot{x}^* - \alpha A x$ and $\Psi = k_1 s + k_2 D^{\gamma} \mathrm{sgn}(s)$. Then we have

$$u = (\alpha B)^{-1}(\Phi + \Psi). \tag{6}$$

3.1.3 Stability analysis

Theorem 1 Subsystem (1) converges asymptotically under the FOISMC Eq. (6), with sliding mode surface (3), if inequality (7) holds:

$$k_{i2d} \geq D_d, \tag{7a}$$

$$k_{i2q} \geq D_q, \tag{7b}$$

$$k_{\omega 2} \geq D_\omega. \tag{7c}$$

Proof The Lyapunov function is selected as

$$V = \frac{1}{2} s^{\mathrm{T}} s.$$

The derivation of the Lyapunov function is obtained as

$$\begin{aligned} \dot{V} &= s^{\mathrm{T}} \dot{s} \\ &= s^{\mathrm{T}}[\beta D^{1-\varepsilon} e + \alpha(\dot{x}^* - Ax - Bu - g(t))] \\ &= -s^{\mathrm{T}} k_1 s - s^{\mathrm{T}}(k_2 D^{\gamma} \mathrm{sgn}(s) + \dot{g}(t)). \end{aligned}$$

The variables s_d, s_q, and s_ω are decoupled with controller (6). The proof of the stability is as follows:

When $s_d \geq 0$, $s_d^{\mathrm{T}}(k_{i2d} D^{\gamma_{id}} \mathrm{sgn}(s_d) + \dot{g}(t)) = s_d^{\mathrm{T}}(k_{i2d} D^{\gamma_{id}} + \dot{g}_{id}(t))$. According to Assumption 1 and inequality (7), this gives $k_{i2d} D^{\gamma_{id}} + \dot{g}_{id}(t) \geq k_{i2d} D^{\gamma_{id}} - \|\dot{g}_{id}(t)\| \geq k_{i2d} - D_d \geq 0$, that is, $s_d^{\mathrm{T}}(k_{i2d} D^{\gamma_{id}} \mathrm{sgn}(s_d) + \dot{g}(t)) \geq 0$.

When $s_d < 0$, $s_d^{\mathrm{T}}(k_{i2d} D^{\gamma_{id}} \mathrm{sgn}(s_d) + \dot{g}(t)) = s_d^{\mathrm{T}}(-k_{i2d} D^{\gamma_{id}} + \dot{g}_{id}(t))$. According to Assumption 1 and inequality (7), this gives $-k_{i2d} D^{\gamma_{id}} + \dot{g}_{id}(t) \leq -k_{i2d} D^{\gamma_{id}} + \|\dot{g}_{id}(t)\| \leq -k_{i2d} + D_d \leq 0$, that is, $s_d^{\mathrm{T}}(k_{i2d} D^{\gamma_{id}} \mathrm{sgn}(s_d) + \dot{g}(t)) \geq 0$.

Therefore, inequality (8) holds:

$$s_d^{\mathrm{T}}(k_{i2d}D^{\gamma_{id}}\mathrm{sgn}(s_d)+\dot{g}(t))\geq 0. \tag{8}$$

Then we have

$$\dot{V}<0.$$

3.2 Intelligent optimization for FOISMC

The speed and position components of PSO were introduced in GWO to improve the optimization (Ma et al., 2021). Based on the flight experience, the velocity and position of each PSO particle can be adaptively adjusted:

$$\begin{aligned} v_i(k+1)=&\zeta\times v_i(k)\\ &+c_{1\mathrm{random}}(0,1)\times(X_{\mathrm{GWO}_1}-p_i(k))\\ &+c_{2\mathrm{random}}(0,1)\times(X_{\mathrm{GWO}_2}-p_i(k))\\ &+c_{3\mathrm{random}}(0,1)\times(X_{\mathrm{GWO}_3}-p_i(k)), \end{aligned} \tag{9}$$

$$p_i(k+1)=p_i(k)+v_i(k+1), \tag{10}$$

where v_i is the gray wolf speed, p_i is the current position of the grey wolf, $c_{1\mathrm{random}}=c_{2\mathrm{random}}=c_{3\mathrm{random}}=0.5$ are the learning factors, ζ is the inertial factor, and X_{GWO_1}, X_{GWO_2}, and X_{GWO_3} are the distance vectors of ω_{GWO} relative to α_{GWO}, β_{GWO}, and δ_{GWO}, respectively.

A better optimization effect can be obtained by introducing the PSO velocity and position components to GWO. For the flow chart of the VGWO algorithm, readers can refer to Ma et al. (2021). The gray wolf population is set to 30 and the maximum number of iterations is set to 150. The fitness function is designed as follows:

$$\text{Minimize } J=\int_0^t t|e_\omega(t)|\mathrm{d}t, \tag{11}$$

where e_ω is the rotor speed tracking error and $e_\omega=\omega^*-\omega$.

4 Improved cascade observer design

The observer consists of ASMO and EHGO.

4.1 ASMO design

Let

$$\begin{bmatrix}E_\alpha\\E_\beta\end{bmatrix}=\begin{bmatrix}-\psi_{\mathrm{f}}\omega_{\mathrm{e}}\sin\theta_{\mathrm{e}}\\ \psi_{\mathrm{f}}\omega_{\mathrm{e}}\cos\theta_{\mathrm{e}}\end{bmatrix}, \tag{12}$$

where ψ_{f} is the flux linkage, and ω_{e} and θ_{e} are the electrical rotor speed and electrical rotor position, respectively.

$$\theta_{\mathrm{e}}=\int\omega_{\mathrm{e}}\mathrm{d}t=\int n_{\mathrm{p}}\omega\mathrm{d}t=n_{\mathrm{p}}\theta,$$

where n_{p} is the number of pole pairs and θ is the rotor position.

In a control cycle, the change of the rotor speed is very small. In other words, the derivative of the electrical rotor speed is nearly zero. The first derivative of Eq. (12) can be obtained as follows:

$$\begin{bmatrix}\dot{E}_\alpha\\\dot{E}_\beta\end{bmatrix}=\begin{bmatrix}-\omega_{\mathrm{e}}E_\beta\\ \omega_{\mathrm{e}}E_\alpha\end{bmatrix}. \tag{13}$$

According to the stationary coordinate system, the structure of the ASMO is

$$\begin{aligned} \frac{\mathrm{d}}{\mathrm{d}t}\begin{bmatrix}\hat{i}_\alpha\\\hat{i}_\beta\end{bmatrix}=&\begin{bmatrix}-\frac{R_{\mathrm{s}}}{L_{\mathrm{s}}}&0\\0&-\frac{R_{\mathrm{s}}}{L_{\mathrm{s}}}\end{bmatrix}\begin{bmatrix}\hat{i}_\alpha\\\hat{i}_\beta\end{bmatrix}\\ &+\begin{bmatrix}\frac{1}{L_{\mathrm{s}}}&0\\0&\frac{1}{L_{\mathrm{s}}}\end{bmatrix}\left(\begin{bmatrix}u_\alpha\\u_\beta\end{bmatrix}-\begin{bmatrix}\hat{E}_\alpha\\\hat{E}_\beta\end{bmatrix}\right)-\frac{\phi}{L_{\mathrm{s}}}\mathrm{sgn}(S), \end{aligned} \tag{14}$$

where $\phi=\mathrm{diag}(\phi_{11},\phi_{22})$ is the ASMO gain, S is the sliding surface of the ASMO, R_{s} is the stator resistance, L_{s} is the stator inductance, i_α and i_β are the α- and β-axis stator currents respectively, and u_α and u_β are the α- and β-axis stator voltages, respectively.

According to Eq. (13), the adaptive law is designed as follows:

$$\begin{bmatrix}\dot{\hat{E}}_\alpha\\\dot{\hat{E}}_\beta\end{bmatrix}=\begin{bmatrix}-\hat{\omega}_{\mathrm{e}}\hat{E}_\beta-\xi\tilde{E}_\alpha\\ \hat{\omega}_{\mathrm{e}}\hat{E}_\alpha-\xi\tilde{E}_\beta\end{bmatrix}, \tag{15}$$

where ξ is a positive number. The manifold S is defined as

$$S=[S_1,S_2]^{\mathrm{T}}=[\hat{i}_\alpha-i_\alpha,\hat{i}_\beta-i_\beta]^{\mathrm{T}}. \tag{16}$$

The observer error is as follows:

$$\begin{aligned} \frac{\mathrm{d}}{\mathrm{d}t}\begin{bmatrix}\tilde{i}_\alpha\\\tilde{i}_\beta\end{bmatrix}=&\begin{bmatrix}-\frac{R_{\mathrm{s}}}{L_{\mathrm{s}}}&0\\0&-\frac{R_{\mathrm{s}}}{L_{\mathrm{s}}}\end{bmatrix}\begin{bmatrix}\tilde{i}_\alpha\\\tilde{i}_\beta\end{bmatrix}\\ &+\begin{bmatrix}\frac{1}{L_{\mathrm{s}}}&0\\0&\frac{1}{L_{\mathrm{s}}}\end{bmatrix}\begin{bmatrix}\tilde{E}_\alpha\\\tilde{E}_\beta\end{bmatrix}-\frac{\phi}{L_{\mathrm{s}}}\mathrm{sgn}(S), \end{aligned} \tag{17}$$

where $\tilde{i}_\alpha=\hat{i}_\alpha-i_\alpha$, $\tilde{i}_\beta=\hat{i}_\beta-i_\beta$, $\tilde{E}_\alpha=\hat{E}_\alpha-E_\alpha$, and $\tilde{E}_\beta=\hat{E}_\beta-E_\beta$.

When $S=0$, the following equation holds:

$$\begin{bmatrix}\tilde{E}_\alpha\\ \tilde{E}_\beta\end{bmatrix}=\begin{bmatrix}\hat{E}_\alpha-E_\alpha\\ \hat{E}_\beta-E_\beta\end{bmatrix}=-\phi\mathrm{sgn}(S). \tag{18}$$

According to Eqs. (13)–(18), the ASMO structure is as follows:

$$\begin{aligned}\frac{\mathrm{d}}{\mathrm{d}t}\begin{bmatrix}\hat{i}_\alpha\\ \hat{i}_\beta\\ \hat{E}_\alpha\\ \hat{E}_\beta\end{bmatrix}=&\begin{bmatrix}-\frac{R_\mathrm{s}}{L_\mathrm{s}} & 0 & -\frac{1}{L_\mathrm{s}} & 0\\ 0 & -\frac{R_\mathrm{s}}{L_\mathrm{s}} & 0 & -\frac{1}{L_\mathrm{s}}\\ 0 & 0 & 0 & -\hat{\omega}_\mathrm{e}\\ 0 & 0 & \hat{\omega}_\mathrm{e} & 0\end{bmatrix}\begin{bmatrix}\hat{i}_\alpha\\ \hat{i}_\beta\\ \hat{E}_\alpha\\ \hat{E}_\beta\end{bmatrix}\\ &+\begin{bmatrix}\frac{1}{L_\mathrm{s}} & 0\\ 0 & \frac{1}{L_\mathrm{s}}\\ 0 & 0\\ 0 & 0\end{bmatrix}\begin{bmatrix}u_\alpha\\ u_\beta\end{bmatrix}+\begin{bmatrix}-\frac{1}{L_\mathrm{s}} & 0\\ 0 & -\frac{1}{L_\mathrm{s}}\\ \xi & 0\\ 0 & \xi\end{bmatrix}\mathrm{sgn}(S).\end{aligned} \tag{19}$$

4.2 Stability analysis

The Lyapunov function is selected as

$$V=\frac{1}{2}\tilde{E}_\alpha^2+\frac{1}{2}\tilde{E}_\beta^2+\frac{1}{2}\tilde{\omega}_\mathrm{e}^2, \tag{20}$$

where $\tilde{\omega}_\mathrm{e}=\hat{\omega}_\mathrm{e}-\omega_\mathrm{e}$.

The difference between Eqs. (13) and (15) is as follows:

$$\begin{bmatrix}\dot{\tilde{E}}_\alpha\\ \dot{\tilde{E}}_\beta\end{bmatrix}=\begin{bmatrix}\dot{\hat{E}}_\alpha-\dot{E}_\alpha\\ \dot{\hat{E}}_\beta-\dot{E}_\beta\end{bmatrix}=\begin{bmatrix}-\hat{\omega}_\mathrm{e}\hat{E}_\beta+\omega_\mathrm{e}E_\beta-\xi\tilde{E}_\alpha\\ \hat{\omega}_\mathrm{e}\hat{E}_\alpha-\omega_\mathrm{e}E_\alpha-\xi\tilde{E}_\beta\end{bmatrix}. \tag{21}$$

The derivation of Eq. (20) is as follows:

$$\begin{aligned}\dot{V}=&\tilde{E}_\alpha(-\hat{\omega}_\mathrm{e}\hat{E}_\beta+\omega_\mathrm{e}E_\beta-\xi\tilde{E}_\alpha)\\ &+\tilde{E}_\beta(\hat{\omega}_\mathrm{e}\hat{E}_\alpha-\omega_\mathrm{e}E_\alpha-\xi\tilde{E}_\beta)+(\hat{\omega}_\mathrm{e}-\omega_\mathrm{e})\frac{\mathrm{d}\tilde{\omega}_\mathrm{e}}{\mathrm{d}t}\\ =&\hat{\omega}_\mathrm{e}\left(\tilde{E}_\beta\hat{E}_\alpha-\tilde{E}_\alpha\hat{E}_\beta+\frac{\mathrm{d}\tilde{\omega}_\mathrm{e}}{\mathrm{d}t}\right)\\ &+\omega_\mathrm{e}\left(\tilde{E}_\alpha E_\beta-\tilde{E}_\beta\hat{E}_\alpha-\frac{\mathrm{d}\tilde{\omega}_\mathrm{e}}{\mathrm{d}t}\right)-\xi(\tilde{E}_\alpha^2+\tilde{E}_\beta^2).\end{aligned} \tag{22}$$

From Eq. (22), $-\xi(\tilde{E}_\alpha^2+\tilde{E}_\beta^2)<0$ can be obtained. According to the Lyapunov stability theory, ASMO is stable when Eq. (23) holds:

$$\begin{cases}\tilde{E}_\beta\hat{E}_\alpha-\tilde{E}_\alpha\hat{E}_\beta+\dfrac{\mathrm{d}\tilde{\omega}_\mathrm{e}}{\mathrm{d}t}=0,\\ \tilde{E}_\alpha E_\beta-\tilde{E}_\beta E_\alpha-\dfrac{\mathrm{d}\tilde{\omega}_\mathrm{e}}{\mathrm{d}t}=0.\end{cases} \tag{23}$$

According to Eq. (23), the estimated rotor speed can be obtained as follows:

$$\frac{\mathrm{d}\hat{\omega}_\mathrm{e}}{\mathrm{d}t}=\tilde{E}_\alpha\hat{E}_\beta-\tilde{E}_\beta\hat{E}_\alpha. \tag{24a}$$

When Eq. (24a) is used to observe the rotor information, the response speed is low. To improve the response speed, Eq. (24a) is modified as follows:

$$\begin{aligned}\hat{\omega}_\mathrm{e}=&\int\dot{\hat{\omega}}_\mathrm{e}\mathrm{d}t=k_\mathrm{pro}(\tilde{E}_\alpha\hat{E}_\beta-\tilde{E}_\beta\hat{E}_\alpha)\\ &+k_\mathrm{int}\int(\tilde{E}_\alpha\hat{E}_\beta-\tilde{E}_\beta\hat{E}_\alpha)\mathrm{d}t,\end{aligned} \tag{24b}$$

where k_pro and k_int are the adjustable gains, and the adjustment process of k_pro and k_int is similar to the PI parameter adjustment process. The estimate of the rotor position is as follows:

$$\hat{\theta}_\mathrm{e}=\int\hat{\omega}_\mathrm{e}\mathrm{d}t. \tag{25}$$

The schematic of the ASMO is shown in Fig. 2, which corresponds to Eqs. (12)–(19).

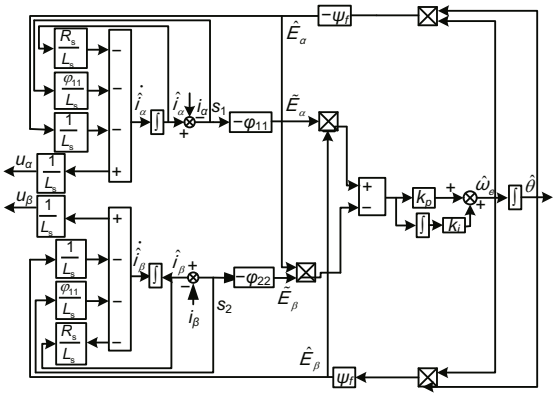

Fig. 2 Schematic of the ASMO

4.3 EHGO design

Based on mechanical motion, EHGO is taken as

$$\begin{cases}\dot{\hat{\vartheta}}_\mathrm{e}=\hat{\omega}_\mathrm{e}+\dfrac{\alpha_1}{\epsilon}(\hat{\theta}_\mathrm{e}-\hat{\vartheta}_\mathrm{e}),\\ \dot{\hat{\omega}}_\mathrm{e}=\dfrac{3n_p^2}{2J}\psi_\mathrm{f}i_q-\dfrac{B_\mathrm{m}}{J}\hat{\omega}_\mathrm{e}+\dfrac{\alpha_2}{\epsilon^2}(\hat{\theta}_\mathrm{e}-\hat{\vartheta}_\mathrm{e})+\hat{\sigma},\\ \hat{\sigma}=\dfrac{\alpha_3}{\epsilon^3}(\hat{\theta}_\mathrm{e}-\hat{\vartheta}_\mathrm{e}),\end{cases} \tag{26}$$

where $\hat{\vartheta}_\mathrm{e}$ and $\hat{\theta}_\mathrm{e}$ are the estimated positions of EHGO and DSMO, respectively. For the observer parameters, readers can refer to Ma et al. (2021).

5 Simulation and analysis

The PMSM parameters are given in Table 1. The simulation includes mainly four parts. First, the

controller parameters are optimized by the VGWO algorithm (Fig. 3). Second, the effectiveness of the improved cascade observer is tested (Figs. 4 and 5). Third, the simulation is completed using the FOISMC-FOISMC method (Fig. 6). Finally, considering the uncertainty, PID-PID, ISMC-ISMC, and FOISMC-FOISMC are compared (Figs. 7–10).

5.1 Optimization of controller parameters

Fig. 3 shows the optimization results of various control strategy parameters based on the VGWO algorithm. The optimization value of the FOISMC-FOISMC method is smaller than those of the other control strategies. It not only shows the effectiveness of VGWO, but also proves that the ability of the FOISMC-FOISMC strategy is better than those of PID-PID and ISMC-ISMC. Table 2 shows the parameter optimization results of the FOISMC-FOISMC control strategy.

5.2 Verification of the proposed cascade observer

To demonstrate the superiority of the improved cascade observer (ASMO+EHGO), we compare it with a traditional cascade observer (SMO+EHGO). The actual rotor speed ω is obtained by FOISMC-FOISMC. Figs. 4 and 5 show the rotor speed and the rotor position based on various observers, respectively. The figures show that the improved observer has the best observation accuracy and strongest robustness. The maximum observation rotor speed error of the improved cascade observer is smaller than that of the traditional cascade observer.

Table 1 Parameters of PMSM

Parameter	Unit	Value
Number of pole pairs, n_p		4
Stator inductance, L_s	mH	8.5
Stator resistance, R_s	Ω	2.875
Flux linkage, ψ_f	Wb	0.175
Moment of inertia, J	$\mathrm{kg\cdot m^2}$	0.001
Viscous friction coefficient, B_m	$\mathrm{N\cdot m\cdot s}$	0
DC voltage, U_dc	V	311

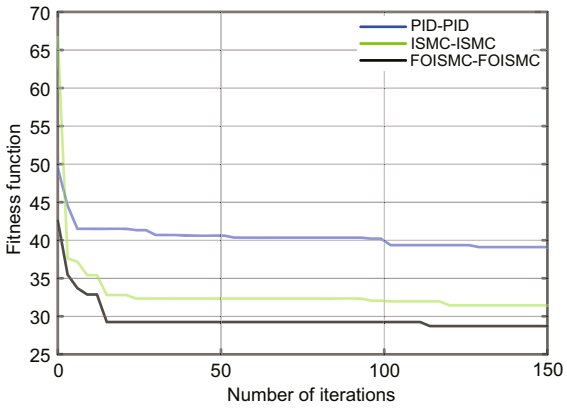

Fig. 3 Optimization results based on VGWO

5.3 Tracking performance simulation

Fig. 6 shows the effect of the employed scheme. The estimated rotor speed ω is obtained using the improved cascade observer (ASMO+EHGO) to estimate the actual ω. Fig. 6a shows that ω can accurately track ω^*. Figs. 6b and 6c show that the improved cascade observer has a high observation

Table 2 Optimization results of the FOISMC-FOISMC based on VGWO

Parameter	Range	Result
α_ω	0–50 000	50 000
α_{id}	0–6000	6000
α_{iq}	0–6000	6000
β_ω	0–10 000	9500
β_{id}	0–1000	1
β_{iq}	0–1000	10
k_{i1d}	0–50 000	5000
k_{i1q}	0–50 000	50 000
$k_{\omega 1}$	0–5000	600
$k_{\omega 2}$	0–5000	5000
k_{i2d}	0–5000	4000
k_{i2q}	0–5000	4000
ε_ω	0–1	0.85
ε_{id}	0–1	0.87
ε_{iq}	0–1	0.87
γ_ω	0–1	0.75
γ_{id}	0–1	0.52
γ_{iq}	0–1	0.53

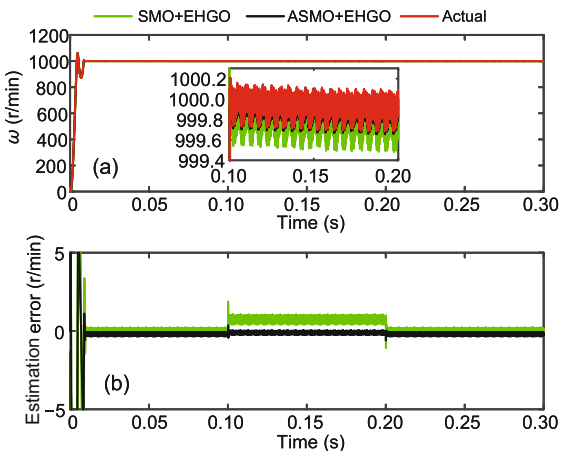

Fig. 4 Comparison of the rotor speed ω (a) and the estimation error (b)

accuracy for rotor speed ω and rotor position θ, respectively. Fig. 6d shows the changes of the load torque T_{L}. As shown in Fig. 6e, the currents i_{a}, i_{b}, and i_{c} are stable.

5.4 Robustness simulation

The following two cases are considered:

Case 1: $\Delta R_{\mathrm{s}}=0$, $\Delta L_{\mathrm{s}}=0$, $\Delta\psi_{\mathrm{f}}=0$.

Case 2: $\Delta R_{\mathrm{s}}=+15\%R_{\mathrm{s}}$, $\Delta L_{\mathrm{s}}=+15\%L_{\mathrm{s}}$, $\Delta\psi_{\mathrm{f}}=+15\%\psi_{\mathrm{f}}$.

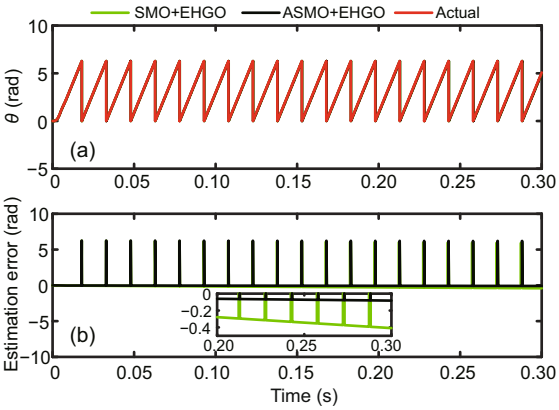

Fig. 5 Comparison of the rotor position θ (a) and the estimation error (b)

Here, ΔR_{s}, ΔL_{s}, and $\Delta\psi_{\mathrm{f}}$ represent the parameter variations of R_{s}, L_{s}, and ψ_{f}, respectively.

For case 1 (Figs. 7 and 8):

Fig. 7 shows that the rotor speed of the FOISMC-FOISMC scheme has a high convergence speed and less chattering. Fig. 8 shows that the currents based on the FOISMC-FOISMC scheme have a smaller tracking error.

The data in Fig. 7 is further processed and is shown in Table 3, from where we can see that the standard deviation of the rotor speed error

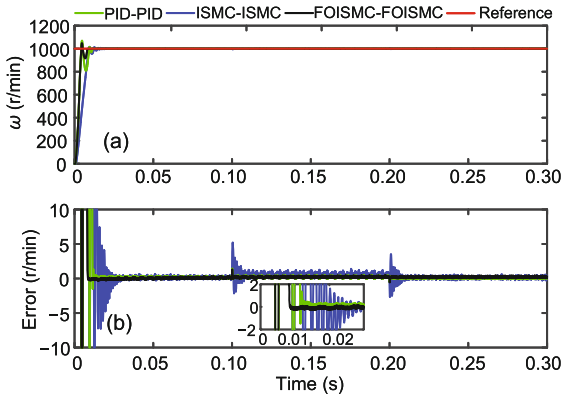

Fig. 7 Comparison of the rotor speed ω (a) and the tracking error (b) for case 1

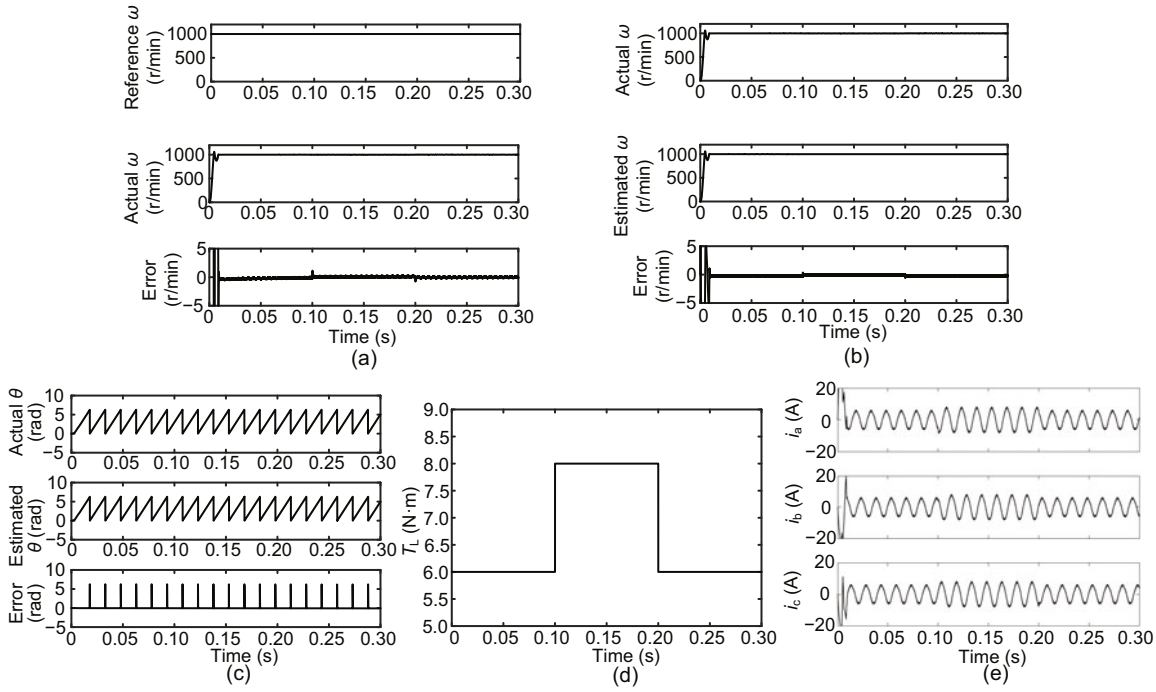

Fig. 6 Tracking performance simulation: (a) rotor speed responses and the tracking error; (b) rotor speed ω estimation and the error; (c) rotor position θ estimation and the error; (d) load torque T_{L}; (e) currents i_{a}, i_{b}, and i_{c}

drops greatly under the FOISMC-FOISMC method. Therefore, the FOISMC-FOISMC strategy can meet high performance requirements.

For case 2 (Figs. 9 and 10):

Figs. 9 and 10 show that the control performance of PID-PID deteriorates significantly compared with the other schemes. These figures show that the robustness of PID-PID is poor, and that FOISMC-FOISMC can significantly reduce chattering and shorten the convergence time. The data in Fig. 9 is further processed and is shown in Table 4. Table 4 shows that the standard deviation of the rotor speed error significantly decreases under the FOISMC-FOISMC method, and that the control effect of the PID-PID strategy deteriorates.

6 Experimental results

Fig. 11 shows the experimental platform (Ma et al., 2021). In this experiment, the reference rotor speed of the PMSM is 1000 r/min. The control effects are compared under the three control strategies. Figs. 12, 13, and 14 show the load torque change, rotor speed tracking, and current response, respectively. The experiment time is set to 120 s.

Fig. 12 shows the load torque change. The PMSM load change is realized by adjusting the voltage of the adjustable power supply. To discuss the

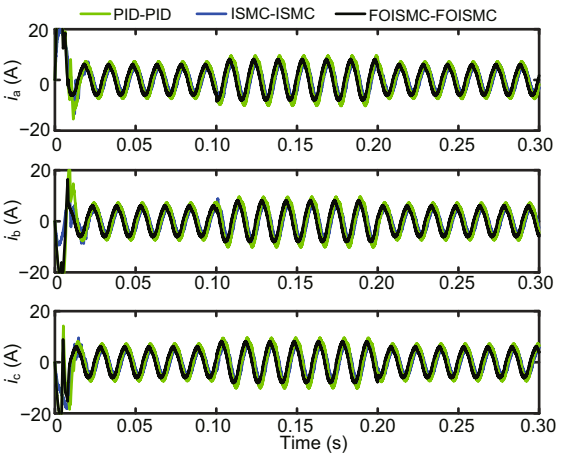

Fig. 8 Currents i_a, i_b, and i_c for case 1

Table 3 Control performance comparison for case 1

Method	Max e_ω	Mean e_ω	Std e_ω
PID-PID	5.21	0.30	0.51
ISMC-ISMC	1.47	0.18	0.17
FOISMC-FOISMC	1.33	0.17	0.13

Unit: r/min

Table 4 Control performance comparison for case 2

Method	Max e_ω	Mean e_ω	Std e_ω
PID-PID	57.42	7.51	23.99
ISMC-ISMC	1.94	0.53	0.23
FOISMC-FOISMC	1.77	0.45	0.16

Unit: r/min

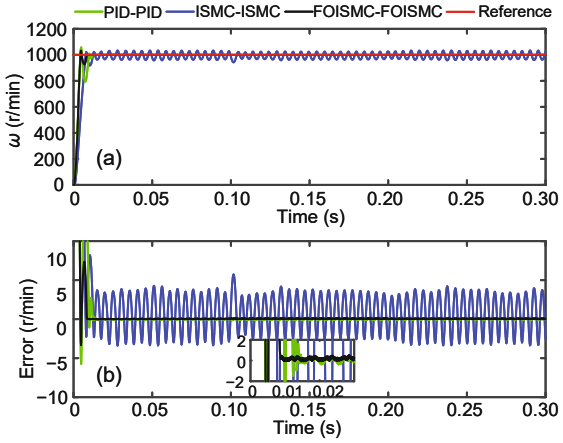

Fig. 9 Comparison of the rotor speed ω (a) and the tracking error (b) for case 2

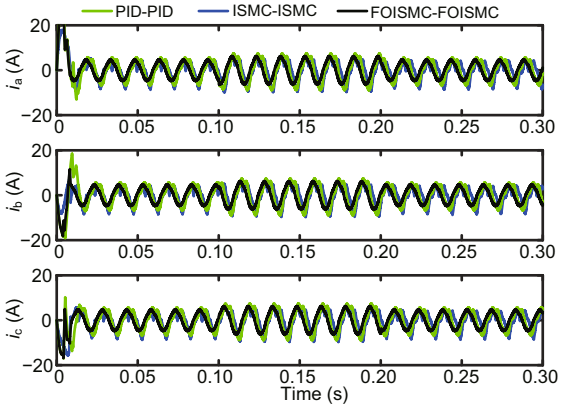

Fig. 10 Currents i_a, i_b, and i_c for case 2

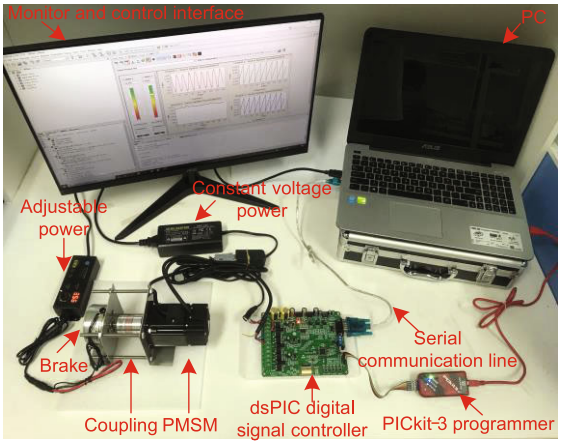

Fig. 11 Experimental platform

effect of the employed algorithm under load change, the torque is adjusted to 0.16 N·m in 0–40 s and 80–120 s, and 0.32 N·m in 40–80 s.

Fig. 13 shows that the PID-PID controller has more fluctuation when the load torque suddenly changes. The figure shows that the FOISMC-FOISMC scheme can achieve better rotor speed tracking and stronger robustness. The data in Fig. 13 is further processed and is shown in Table 5, which shows that the control effect of the PID-PID strategy deteriorates.

Fig. 14 shows that the current changes with the load torque change. The figure shows that the current response of the FOISMC-FOISMC scheme maintains a stable state and has less chattering.

Table 5 Control performance comparison in experiment

Method	Range ω	Mean ω	Std ω
PID-PID	956.11–1063.12	1001.71	17.12
ISMC-ISMC	983.06–1022.91	1000.65	9.95
FOISMC-FOISMC	977.58–1020.84	1000.45	6.43

Unit: r/min

7 Conclusions

Based on model uncertainty and external disturbance, a robust sensorless control scheme was employed. Results showed that the FOISMC-FOISMC strategy has better control performance compared with PID-PID and ISMC-ISMC. In addition, the proposed improved cascade observer has better observation effect, meeting the control requirements. The effectiveness of the strategy was tested by simulations and an experiment. The scheme can be applied to the field of wind power generation. However, the model parameter identification (Fei and Feng, 2020; Fei and Wang, 2020) and an adaptive adjustment algorithm (Fei and Chen, 2020) were not considered in the proposed control strategy. These issues will be addressed in further research, along with the consideration of actuator failures and fault tolerant control (Azizi et al., 2019).

Contributors

Lingfei XIAO and Leiming MA designed the research. Leiming MA drafted the paper. Xinhao HUANG helped organize the paper and polished the English. Lingfei XIAO and Leiming MA revised and finalized the paper.

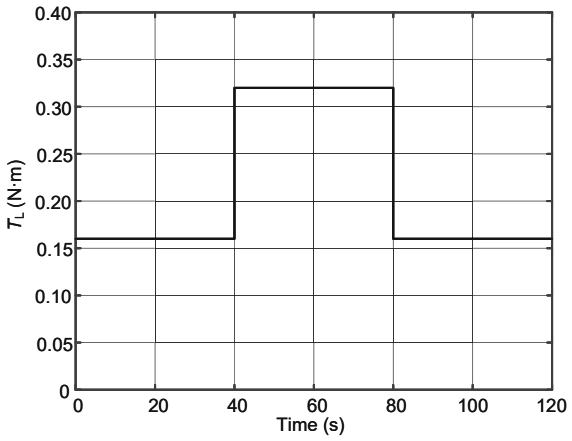

Fig. 12 T_L in the experiment

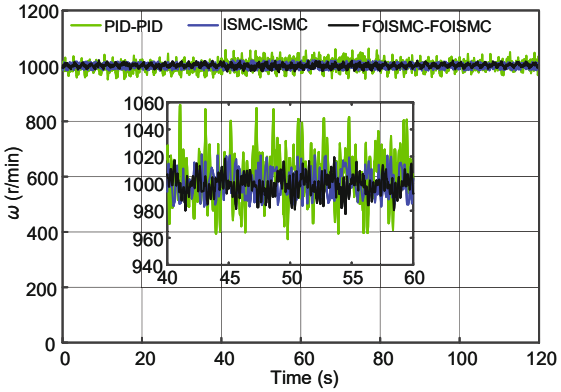

Fig. 13 Rotor speed ω in the experiment

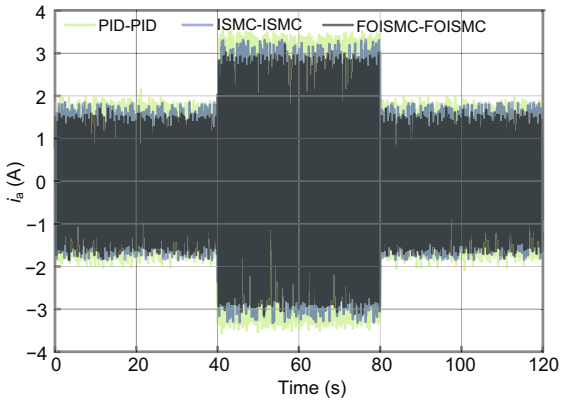

Fig. 14 Current i_a in the experiment

Compliance with ethics guidelines

Lingfei XIAO, Leiming MA, and Xinhao HUANG declare that they have no conflict of interest.

References

Apte A, Thakar U, Joshi V, 2019. Disturbance observer based rotor speed control of PMSM using fractional order PI controller. *IEEE/CAA J Autom Sin*, 6(1):316-326. https://doi.org/10.1109/JAS.2019.1911354

Azizi A, Nourisola H, Shoja-Majidabad S, 2019. Fault tolerant control of wind turbines with an adaptive output feedback sliding mode controller. *Renew Energy*, 135: 55-65. https://doi.org/10.1016/j.renene.2018.11.106

Bakkyaraj T, Sahadevan R, 2015. Invariant analysis of nonlinear fractional ordinary differential equations with Riemann-Liouville fractional derivative. *Nonl Dynam*, 80(1):447-455. https://doi.org/10.1007/s11071-014-1881-4

Fei JT, Chen Y, 2020. Dynamic terminal sliding-mode control for single-phase active power filter using new feedback recurrent neural network. *IEEE Trans Power Electron*, 35(9):9904-9922. https://doi.org/10.1109/TPEL.2020.2974470

Fei JT, Feng ZL, 2020. Fractional-order finite-time super-twisting sliding mode control of micro gyroscope based on double-loop fuzzy neural network. *IEEE Trans Syst Man Cybern Syst*, 51(12):7692-7706. https://doi.org/10.1109/TSMC.2020.2979979

Fei JT, Wang H, 2020. Experimental investigation of recurrent neural network fractional-order sliding mode control of active power filter. *IEEE Trans Circ Syst II*, 67(11):2522-2526. https://doi.org/10.1109/TCSII.2019.2953223

Foo G, Rahman MF, 2010. Sensorless sliding-mode MTPA control of an IPM synchronous motor drive using a sliding-mode observer and HF signal injection. *IEEE Trans Ind Electron*, 57(4):1270-1278. https://doi.org/10.1109/TIE.2009.2030820

Hamida MA, de Leon J, Glumineau A, 2017. Experimental sensorless control for IPMSM by using integral backstepping strategy and adaptive high gain observer. *Contr Eng Pract*, 59:64-76. https://doi.org/10.1016/j.conengprac.2016.11.012

Kivanc OC, Ozturk SB, 2018. Sensorless PMSM drive based on stator feedforward voltage estimation improved with MRAS multiparameter estimation. *IEEE/ASME Trans Mechatron*, 23(3):1326-1337. https://doi.org/10.1109/TMECH.2018.2817246

Ma L, Xiao L, Yang J, et al., 2021. Sensorless intelligent second-order integral sliding mode maximum power point tracking control for wind turbine system based on wind speed estimation. *Proc Inst Mech Eng*, 235(7):1046-1063. https://doi.org/10.1177/0959651820982405

MacDonald CL, Bhattacharya N, Sprouse BP, et al., 2015. Efficient computation of the Grünwald-Letnikov fractional diffusion derivative using adaptive time step memory. *J Comput Phys*, 297:221-236. https://doi.org/10.1016/j.jcp.2015.04.048

Mirjalili S, Mirjalili SM, Lewis A, 2014. Grey wolf optimizer. *Adv Eng Softw*, 69:46-61. https://doi.org/10.1016/j.advengsoft.2013.12.007

Nguyen AT, Rafaq MS, Choi HH, et al., 2018. A model reference adaptive control based speed controller for a surface-mounted permanent magnet synchronous motor drive. *IEEE Trans Ind Electron*, 65(12):9399-9409. https://doi.org/10.1109/TIE.2018.2826480

Pan I, Das S, 2016. Fractional order fuzzy control of hybrid power system with renewable generation using chaotic PSO. *ISA Trans*, 62:19-29. https://doi.org/10.1016/j.isatra.2015.03.003

Poli R, Kennedy J, Blackwell T, 2007. Particle swarm optimization. *Swarm Intell*, 1:33-57. https://doi.org/10.1007/s11721-007-0002-0

Shi TN, Wang Z, Xia CL, 2015. Speed measurement error suppression for PMSM control system using self-adaption Kalman observer. *IEEE Trans Ind Electron*, 62(5):2753-2763. https://doi.org/10.1016/j.isatra.2015.03.003

Thakar U, Joshi V, Vyawahare V, 2017. Design of fractional-order PI controllers and comparative analysis of these controllers with linearized, nonlinear integer-order and nonlinear fractional-order representations of PMSM. *Int J Dynam Contr*, 5(1):187-197. https://doi.org/10.1007/s40435-016-0243-0

Tran DC, Wu ZJ, Wang ZL, et al., 2015. A novel hybrid data clustering algorithm based on artificial bee colony algorithm and K-means. *Chin J Electron*, 24(4):694-701. https://doi.org/10.1049/cje.2015.10.006

Waheed A, Rehman AU, Qureshi MI, et al., 2019. On Caputo k-fractional derivatives and associated inequalities. *IEEE Access*, 7:32137-32145. https://doi.org/10.1109/ACCESS.2019.2902317

Wang Y, Geng L, Hao WJ, et al., 2018. Control method for optimal dynamic performance of DTC-based PMSM drives. *IEEE Trans Energy Conver*, 33(3):1285-1296. https://doi.org/10.1109/TEC.2018.2794527

Wu SF, Zhang JW, 2018. A terminal sliding mode observer based robust backstepping sensorless speed control for interior permanent magnet synchronous motor. *Int J Contr Autom Syst*, 16(6):2743-2753. https://doi.org/10.1007/s12555-017-0806-7

Xie YL, Tang XQ, Song B, et al., 2018. Data-driven adaptive fractional order PI control for PMSM servo system with measurement noise and data dropouts. *ISA Trans*, 75: 172-188. https://doi.org/10.1016/j.isatra.2018.02.018

Yan JD, Wang H, Huang SD, et al., 2019. Load disturbance observer-based complementary sliding mode control for PMSM of the mine traction electric locomotive. *Int J Fuzzy Syst*, 21(4):1051-1058. https://doi.org/10.1007/s40815-018-0579-z

Yang B, Yu T, Shu HC, et al., 2019. Sliding-mode perturbation observer-based sliding-mode control design for stability enhancement of multi-machine power systems. *Trans Inst Meas Contr*, 41(5):1418-1434. https://doi.org/10.1177/0142331218783240

Zhang HS, Wang P, Han BC, et al., 2014. Rotor position measuring method for magnetic levitation high speed PMSM based on fuzzy sliding mode observer. *Trans China Electrotech Soc*, 29(7):147-153 (in Chinese). https://doi.org/10.3969/j.issn.1000-6753.2014.07.020

Zhao Y, Qiao W, Wu L, 2013. An adaptive quasi-sliding-mode rotor position observer-based sensorless control for interior permanent magnet synchronous machines. *IEEE Trans Power Electron*, 28(12):5618-5629. https://doi.org/10.1109/TPEL.2013.2246871

Zhu AJ, Xu CP, Li Z, et al., 2015. Hybridizing grey wolf optimization with differential evolution for global optimization and test scheduling for 3D stacked SoC. *J Syst Eng Electron*, 26(2):317-328. https://doi.org/10.1109/JSEE.2015.00037